Supplement of Atmos. Chem. Phys., 24, 4001–4015, 2024
https://doi.org/10.5194/acp-24-4001-2024-supplement

Atmospheric Chemistry and Physics
Open Access
EGU

Supplement of

Weakened aerosol–radiation interaction exacerbating ozone pollution in eastern China since China's clean air actions

Hao Yang et al.

Correspondence to: Lei Chen (chenlei@nuist.edu.cn) and Hong Liao (hongliao@nuist.edu.cn)

Table S1. WRF-Chem model configurations with main physical and chemical schemes adopted in this study.

Model set-up	**Values**
Domain	East Asia
Study period	June and December 2017
Domain size	167 × 167
Domain center	34 °N, 108 °E
Horizontal resolution	27 km × 27 km
Vertical resolution	32 eta levels up to 50 hPa
Meteorological boundary and initial conditions	NCEP 1°×1° reanalysis data
Chemical initial and boundary conditions	CAM-Chem output
Physical options	**Adopted scheme**
Microphysics scheme	Lin (Purdue) scheme
Cumulus scheme	Grell 3D ensemble scheme
Boundary layer scheme	Yonsei University PBL scheme
Surface layer scheme	Monin-Obukhov surface scheme
Land-surface scheme	Unified Noah land-surface model
Longwave radiation scheme	RRTMG
Shortwave radiation scheme	RRTMG
Chemical options	**Adopted scheme**
Gas phase chemistry	CBMZ
Aerosols	MOSAIC
Photolysis	Fast-J
Biogenic emissions	MEGAN
Anthropogenic emissions	MEIC

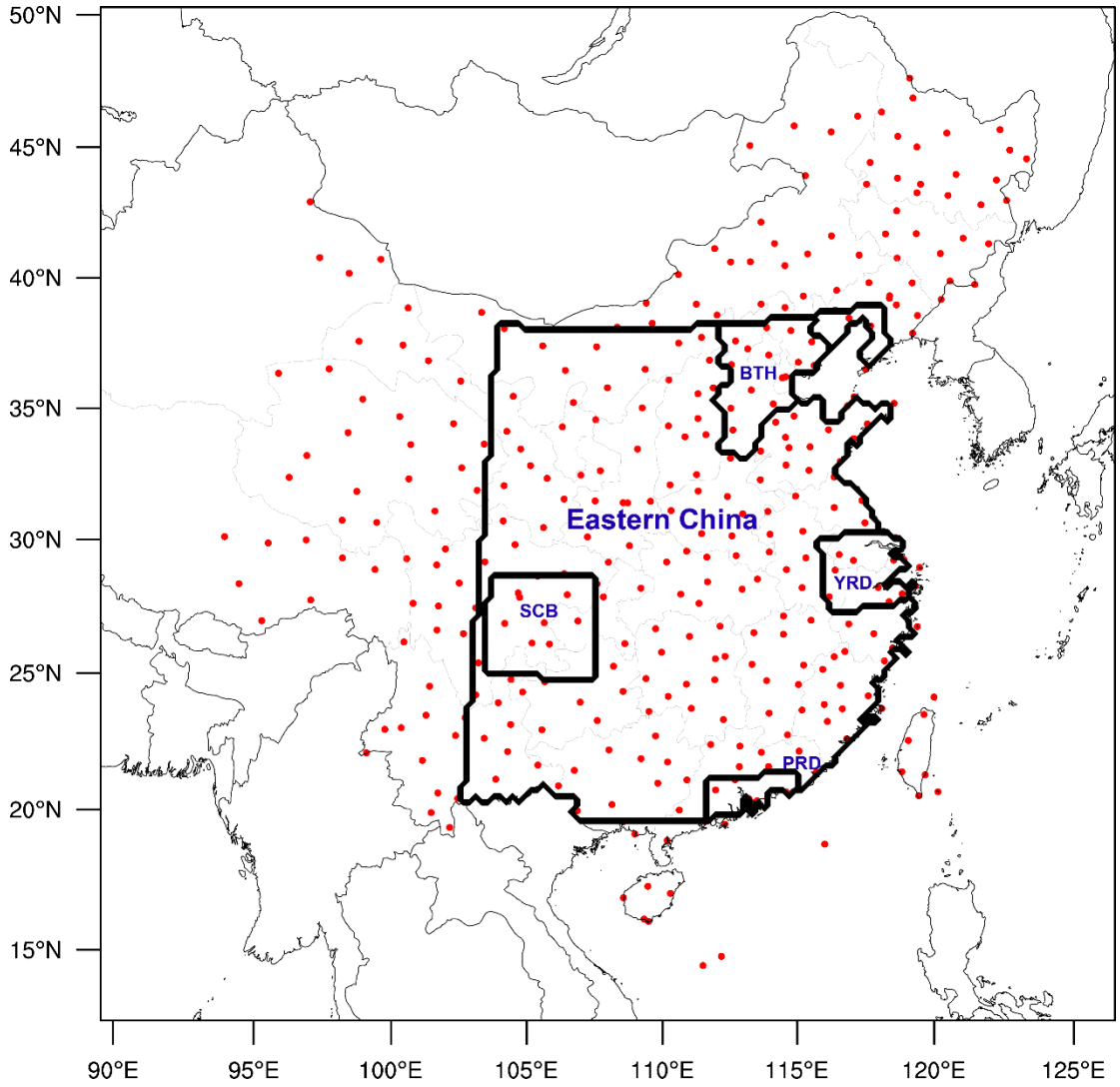

Figure S1. Map of the WRF-Chem simulation domain. Red dots represent meteorological monitoring sites. Five selected regions are also shown in bold black lines, including eastern China, Beijing-Tianjin-Hebei (BTH), Yangtze River Delta (YRD), Pearl River Delta (PRD), and Sichuan Basin (SCB).

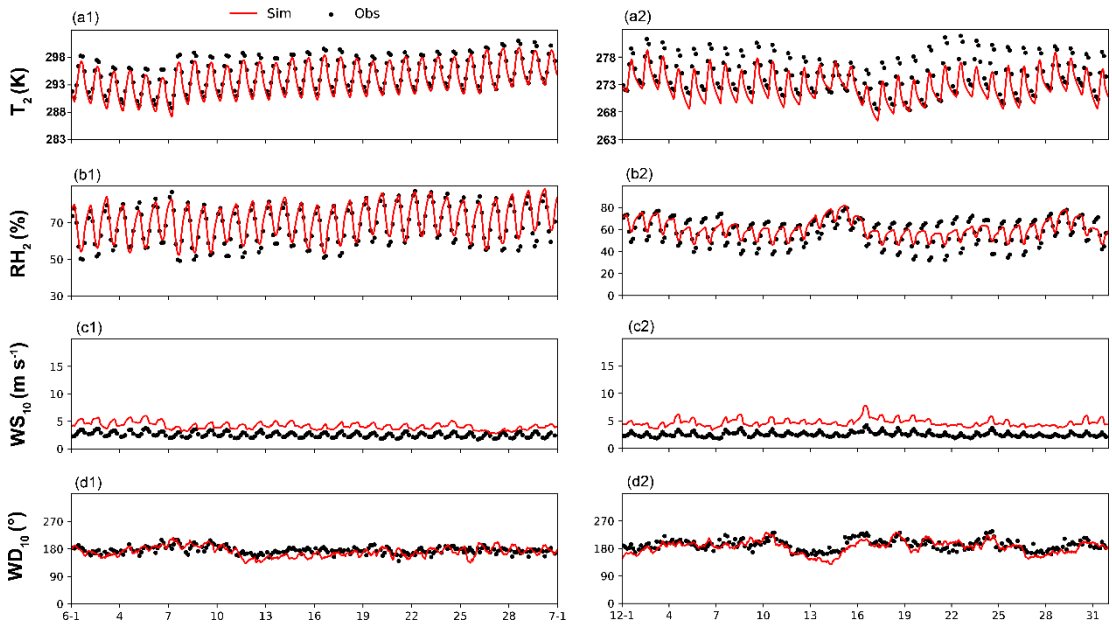

Figure S2. Comparison of 3-hourly observed (black dots) and hourly simulated (red lines) surface meteorological variables of **(a)** 2 m temperature (T_2), **(b)** 2 m relative humidity (RH_2), **(c)** 10 m wind speed (WS_{10}), and **(d)** 10 m wind direction (WD_{10}) averaged over 353 meteorological observation stations during summer (left column) and winter (right column) in 2017.

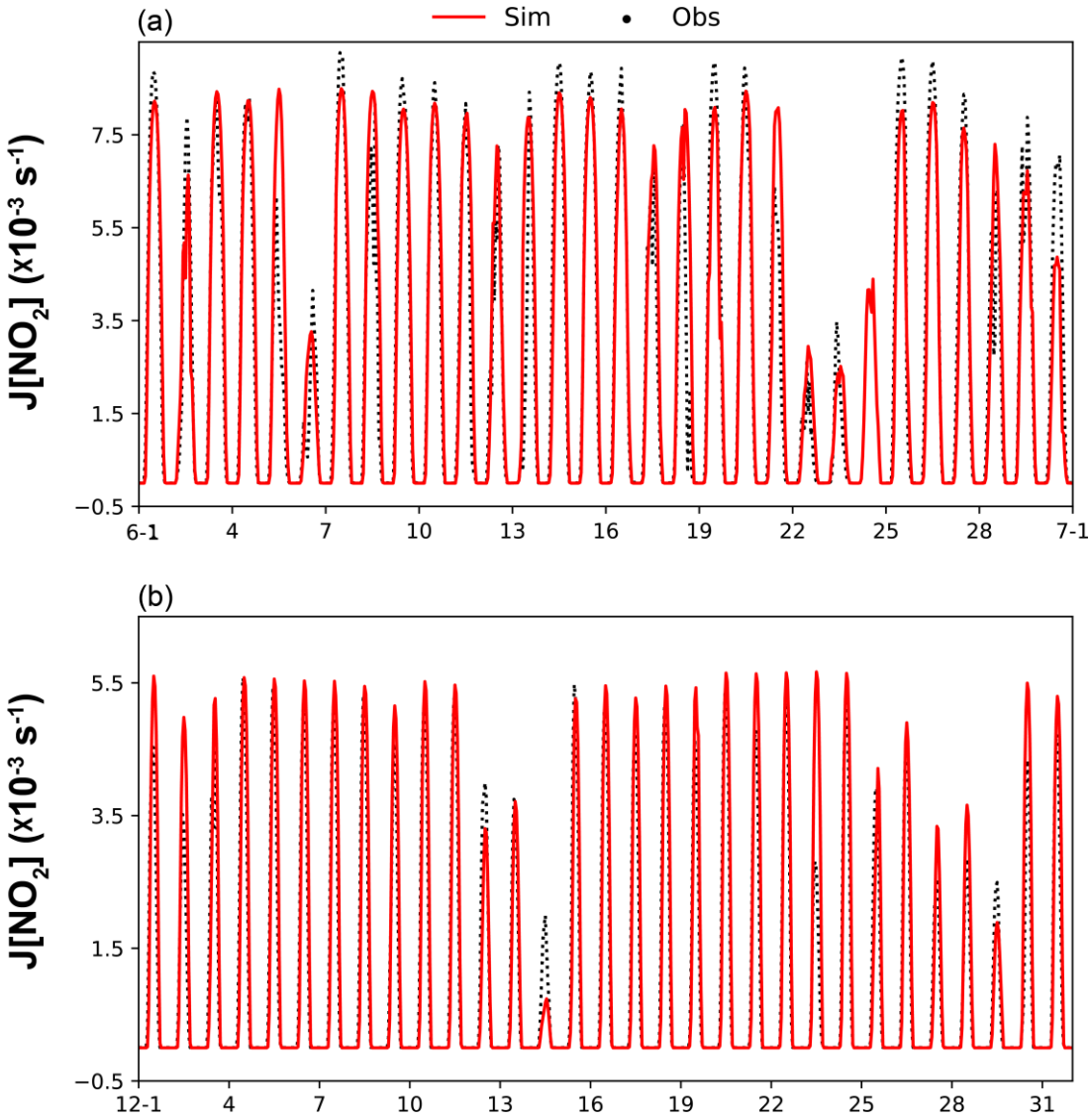

Figure S3. Time series of hourly observed (black dots) and simulated (red lines) surface photolysis rate of NO_2 ($J[NO_2]$) in **(a)** summer and **(b)** winter in 2017.

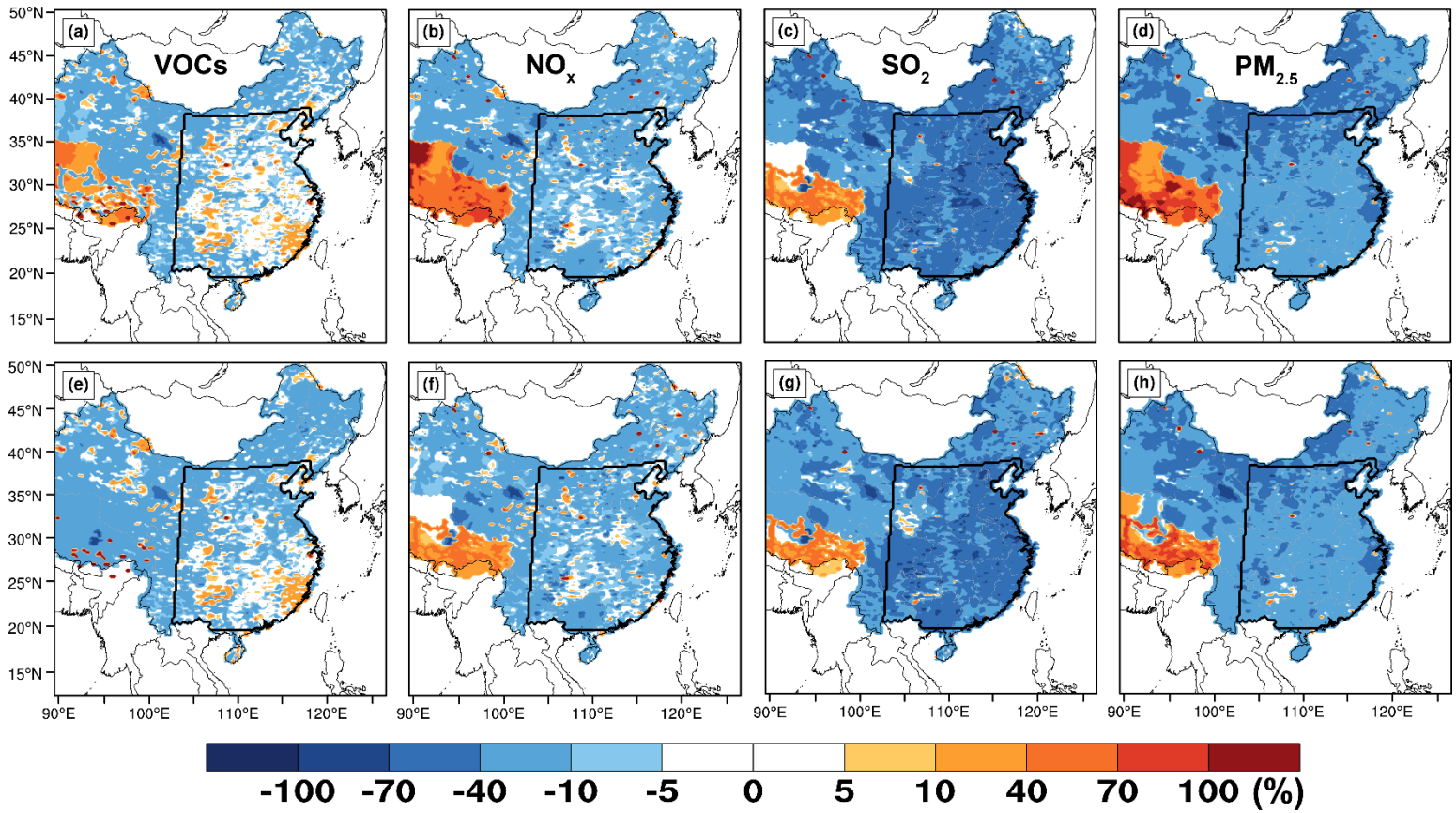

Figure S4. Spatial distributions of changed summer (upper) and winter (bottom) anthropogenic emissions in 2017 relative to that in 2013. **(a, e)** VOCs, **(b, f)** NO_x, **(c, g)** SO_2 and **(d, h)** $PM_{2.5}$. The enclosed black lines represent eastern China.

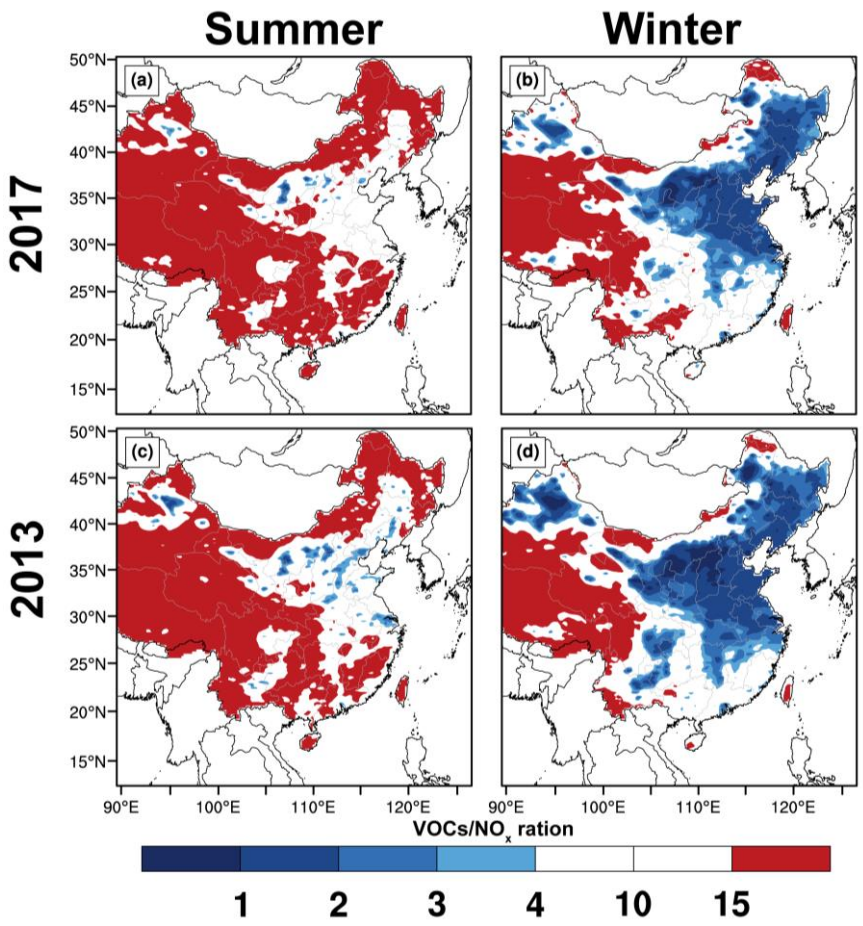

Figure S5. The ratios of VOCs/NO_x calculated from **(a, b)** BASE_17E17M, and **(c, d)** BASE_13E13M during the daytime (08:00-17:00 LST) from summer (left) and winter (right).

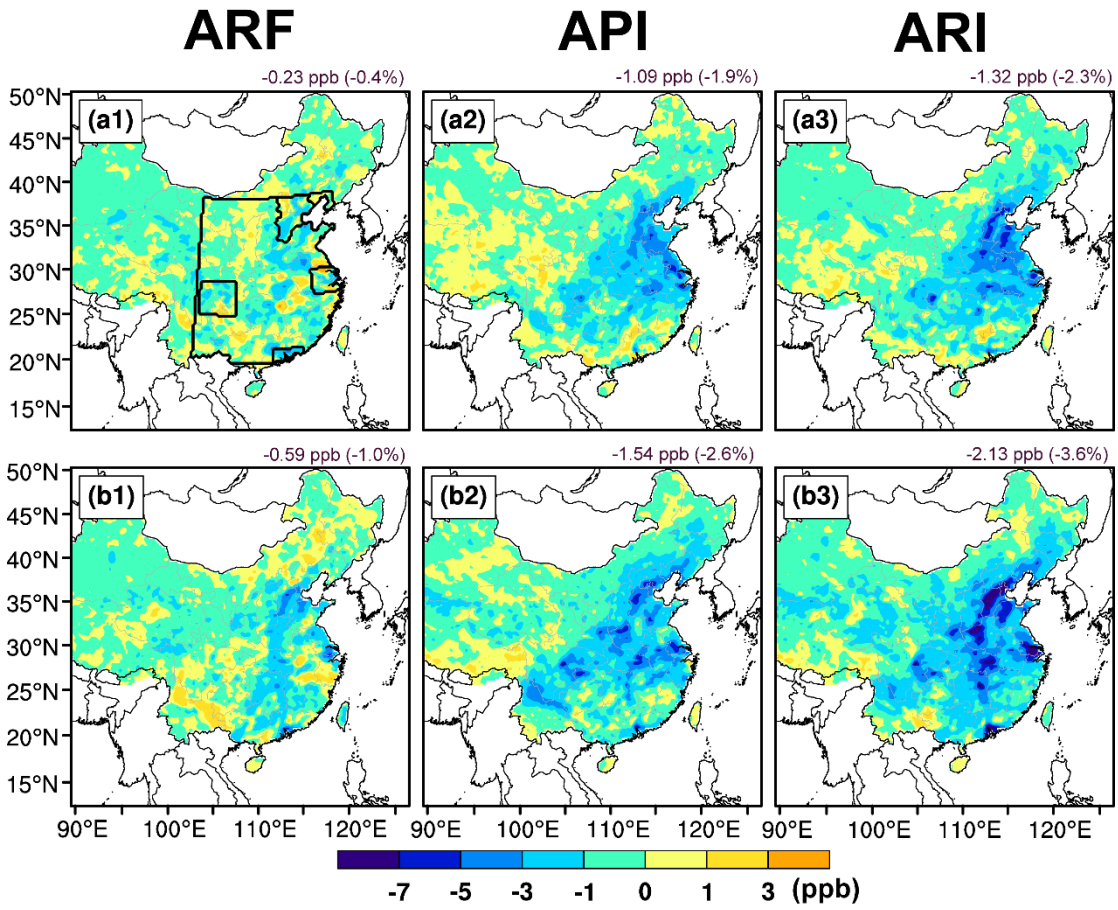

Figure S6. The impacts of **(a1, b1)** aerosol-radiation feedback (ARF), **(a2, b2)** aerosol-photolysis interaction (API), and **(a3, b3)** aerosol-radiation interaction (ARI=ARF+API) on surface-layer MDA8 O_3 in summer under different anthropogenic emission conditions in year 2017 (upper) and year 2013 (bottom).

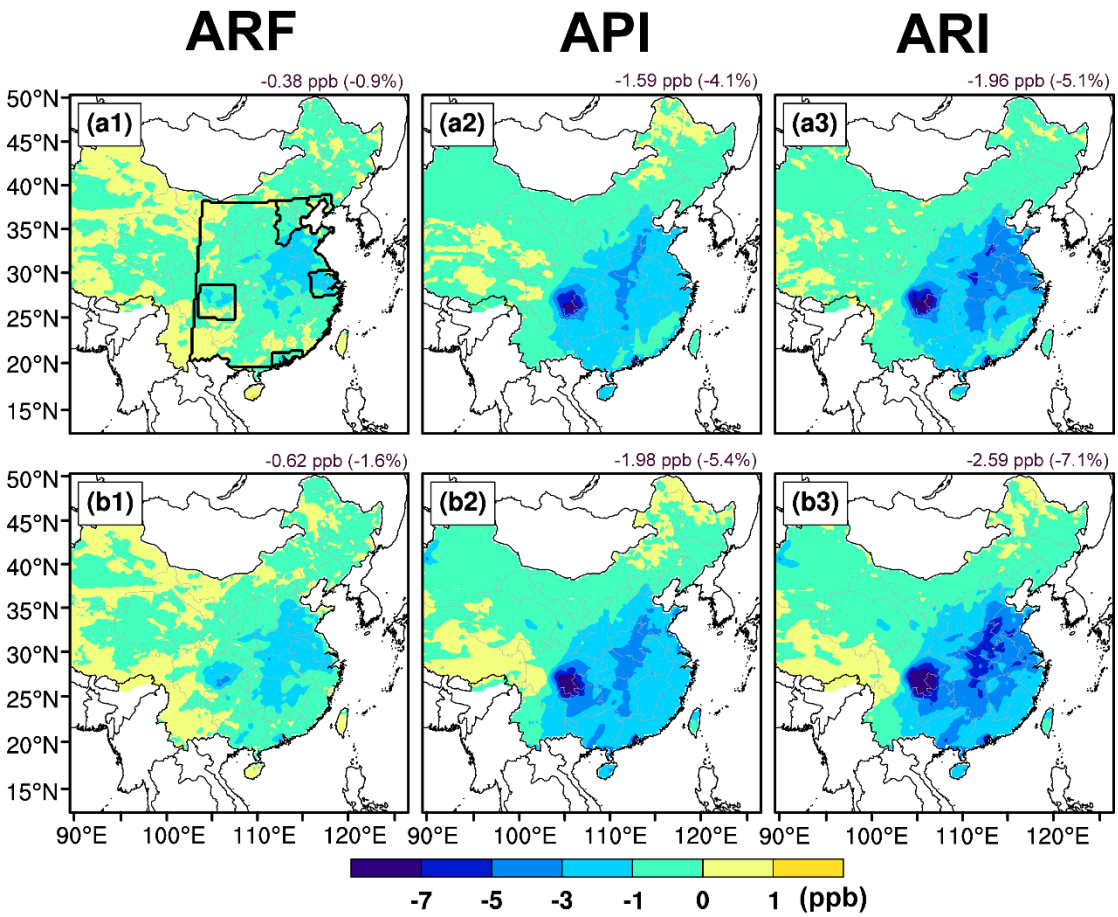

Figure S7. Same as Figure S6 but for winter.

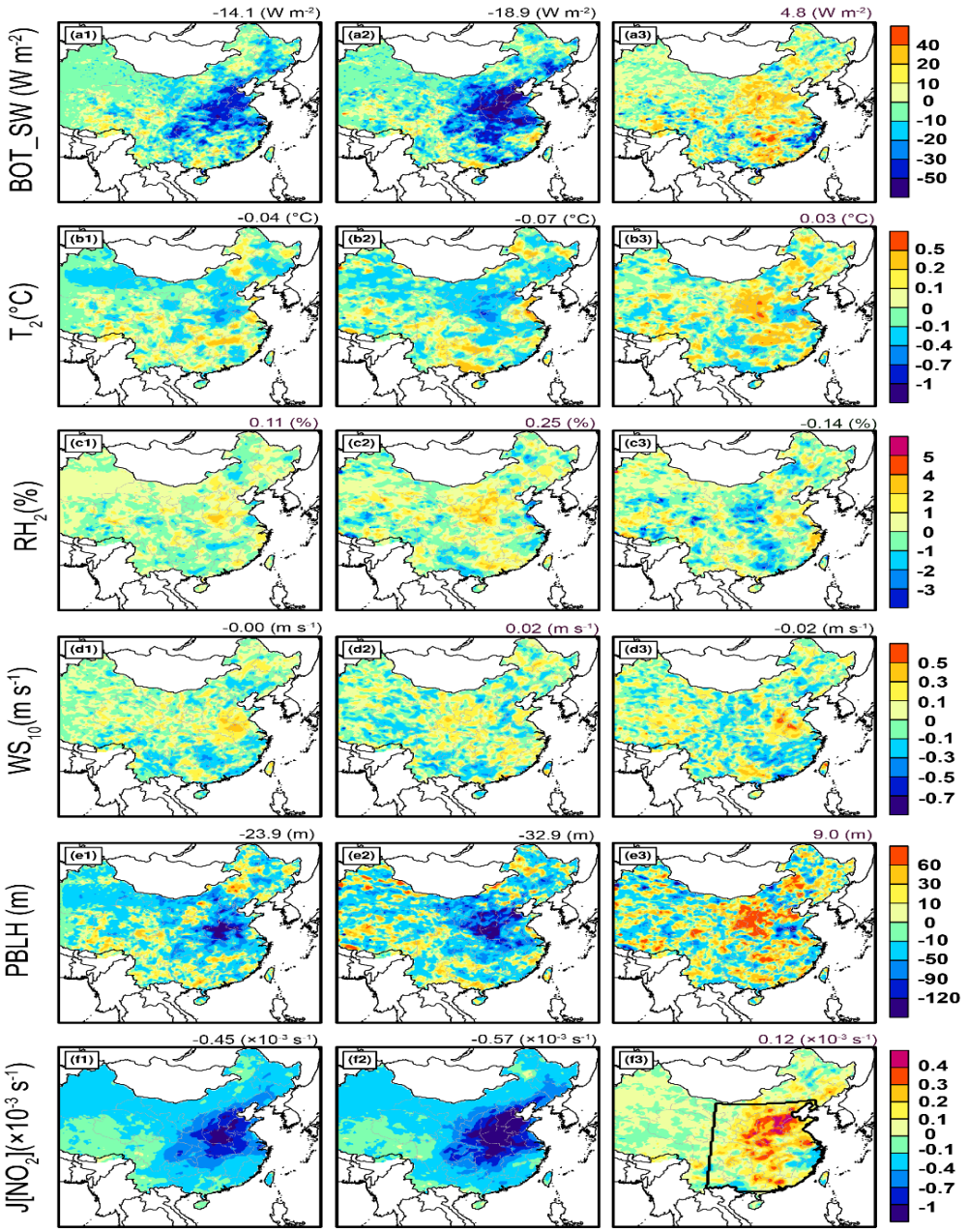

Figure S8. The impacts of aerosol-radiation interaction on **(a)** downward shortwave radiation at the surface (BOT_SW), **(b)** 2-m temperature (T_2), **(c)** 2-m relative humidity (RH_2), **(d)** 10-m wind speed (WS_{10}), **(e)** PBL height (PBLH), and **(f)** J[NO_2] during the daytime (08:00-17:00 LST) in summer. The **(a1-f1)** left panels show the impacts from ΔO_3_ARI_{17E}. The **(a2-f2)** middle panels show the impacts from ΔO_3_ARI_{13E}. The **(a3-f3)** right panels show the impacts from ΔO_3_ΔARI_EMI. Detailed information about ΔO_3_ARI_{17E}, ΔO_3_ARI_{13E}, and ΔO_3_ΔARI_EMI can be found in Figure 1. The enclosed black line in **(f3)** represents eastern China. The mean changes over eastern China are also shown at the top of each panel.

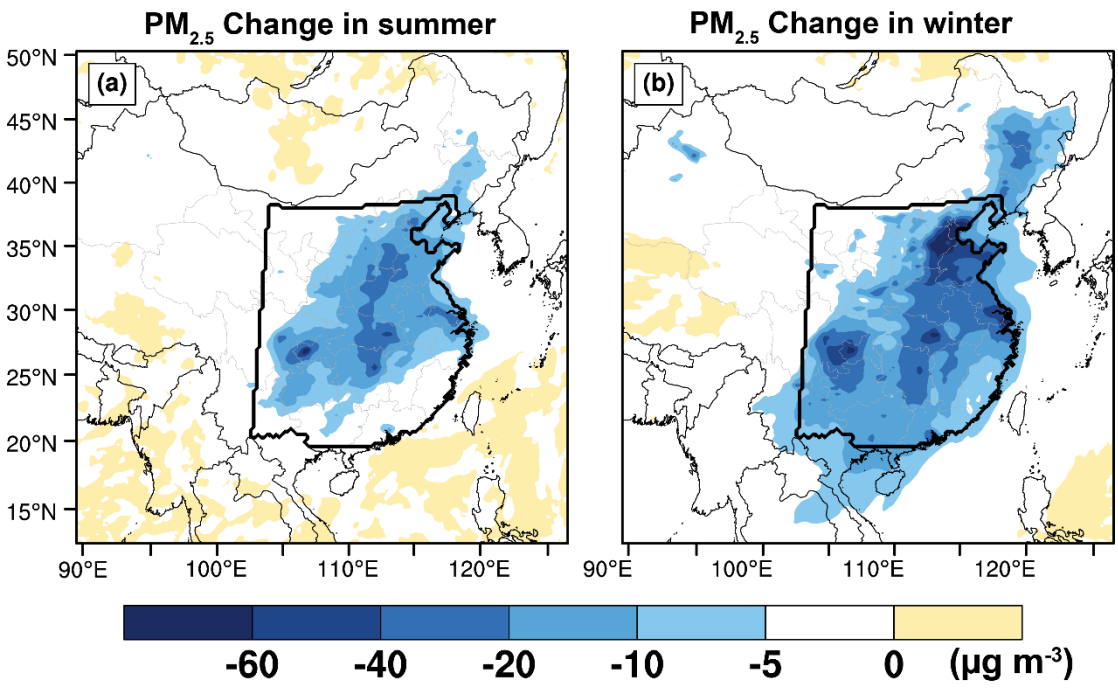

Figure S9. Changes in simulated $PM_{2.5}$ concentrations in **(a)** summer and **(b)** winter from 2013 to 2017 due to anthropogenic emission reductions.

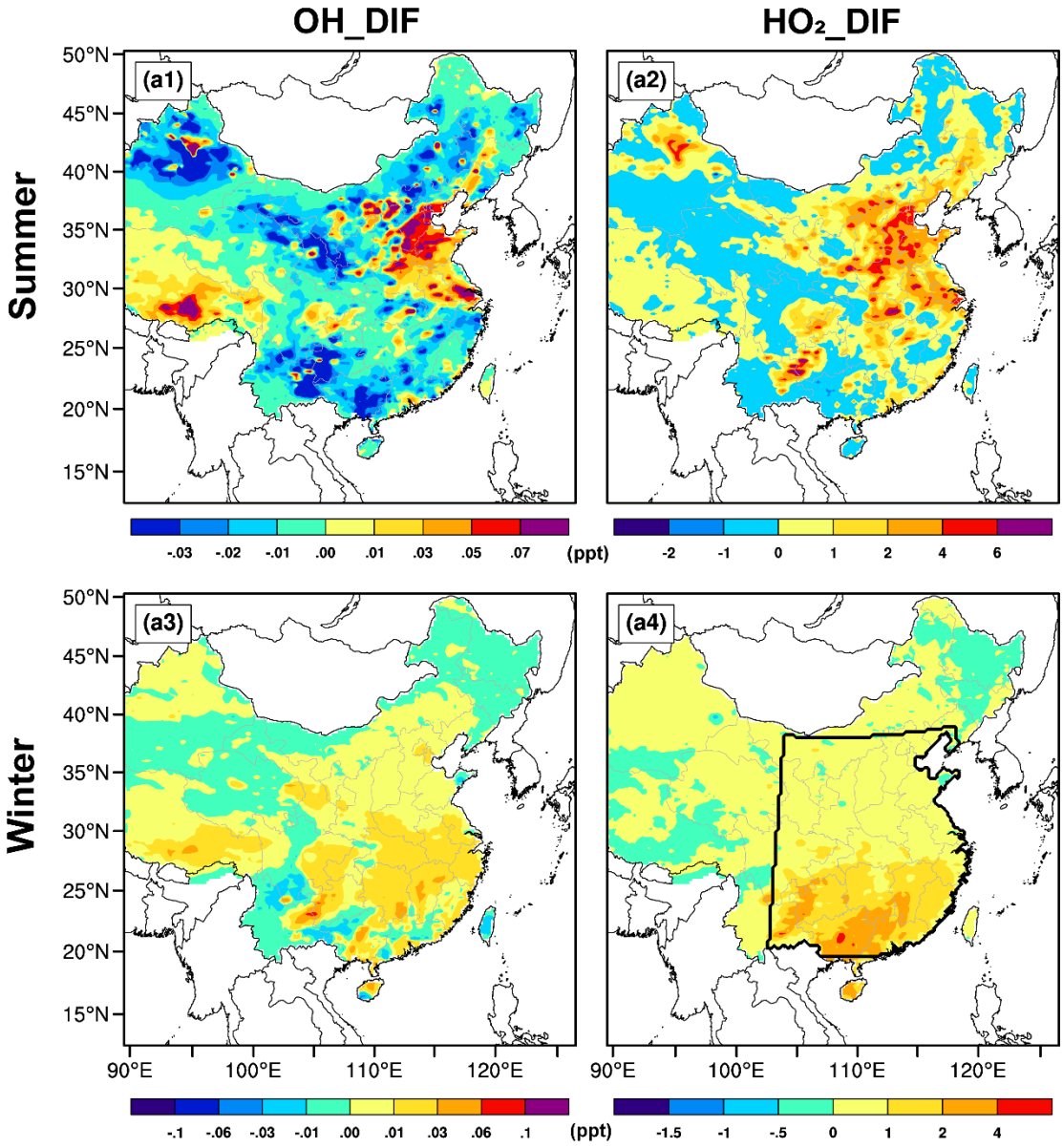

Figure S10. Spatial distribution of changed summer (upper) and winter (bottom) surface-layer **(a1, a3)** OH and **(a2, a4)** HO_2 concentrations from 2013 to 2017 due to anthropogenic emission reductions.

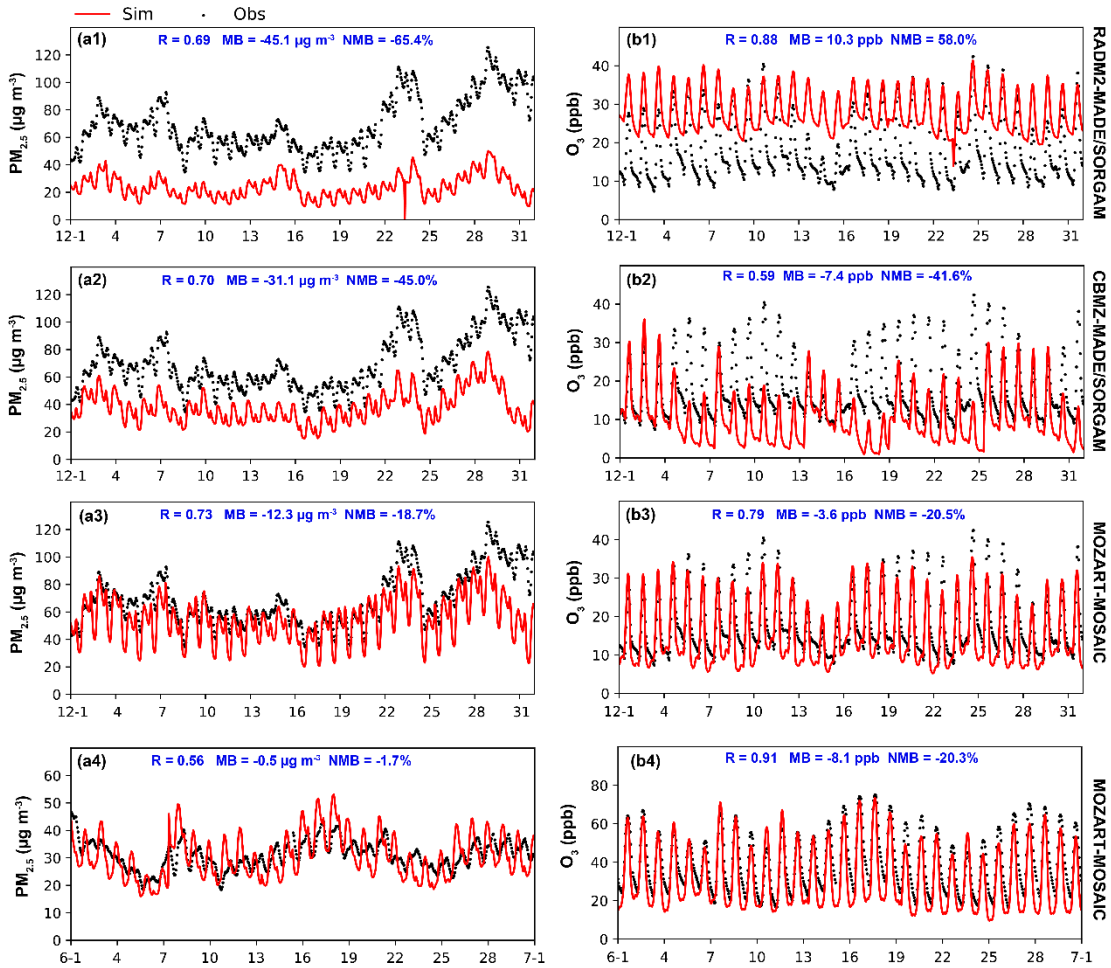

Figure S11. Time series of observed (black dots) and simulated (red lines) hourly **(a1-a4)** $PM_{2.5}$ and **(b1-b4)** O_3 concentrations averaged over the whole observation sites in eastern China during summer and winter 2017. **(a1, b1)** Simulated $PM_{2.5}$ and O_3 concentrations in winter 2017 by RADM2 gas-phase chemistry coupled with MADE/SORGAM aerosol module (RADM2-MADE/SORGAM). **(a2, b2)** Simulated $PM_{2.5}$ and O_3 concentrations in winter 2017 by CBMZ gas-phase chemistry coupled with MADE/SORGAM aerosol module (CBMZ-MADE/SORGAM). **(a3, b3)** Simulated $PM_{2.5}$ and O_3 concentrations in winter 2017 by MOZART gas-phase chemistry coupled with MOSAIC aerosol module (MOZART-MOSAIC). **(a4, b4)** is the same as **(a3, b3)**, but for summer 2017. The calculated correlation coefficient (R), mean bias (MB), and normalized mean bias (NMB) are also shown.

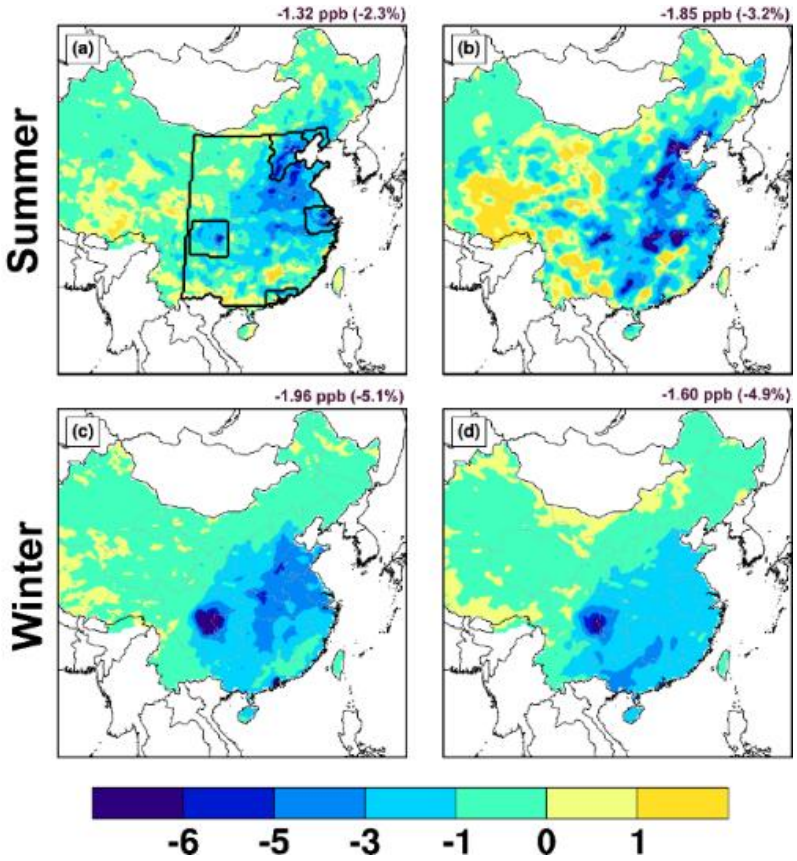

Figure S12. The effects of aerosol-radiation interaction on surface-layer MDA8 O_3 in summer (upper) and winter (bottom) calculated by **(a, c)** CBMZ-MOSAIC and **(b, d)** MOZART-MOSAIC mechanisms. The calculated changes (percentage changes) averaged over China are also shown at the top of each panel.

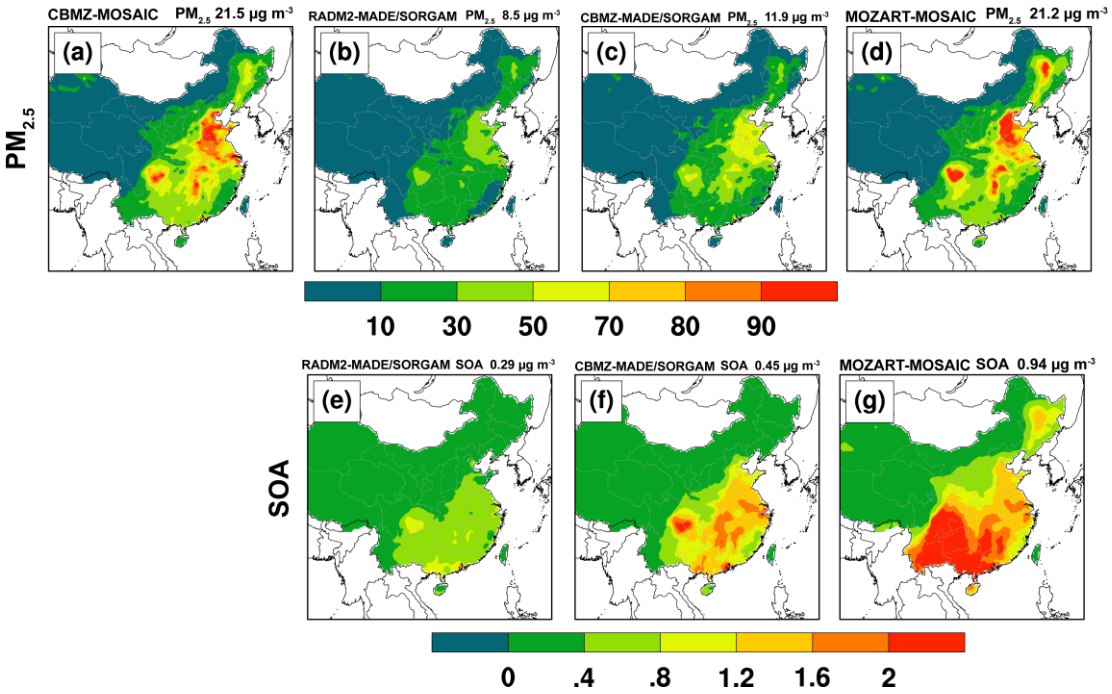

Figure S13. Spatial distributions of simulated mean $PM_{2.5}$ and SOA concentrations (μg m^{-3}) in winter 2017 by **(a)** CBMZ gas-phase chemistry coupled with MOSAIC aerosol module (CBMZ-MOSAIC), **(b, e)** RADM2 gas-phase chemistry coupled with MADE/SORGAM aerosol module (RADM2-MADE/SORGAM), **(c, f)** CBMZ gas-phase chemistry coupled with MADE/SORGAM aerosol module (CBMZ-MADE/SORGAM), and **(d, g)** MOZART gas-phase chemistry coupled with MOSAIC aerosol module (MOZART-MOSAIC). The calculated pollutant concentrations averaged over China are also shown at the top of each panel.

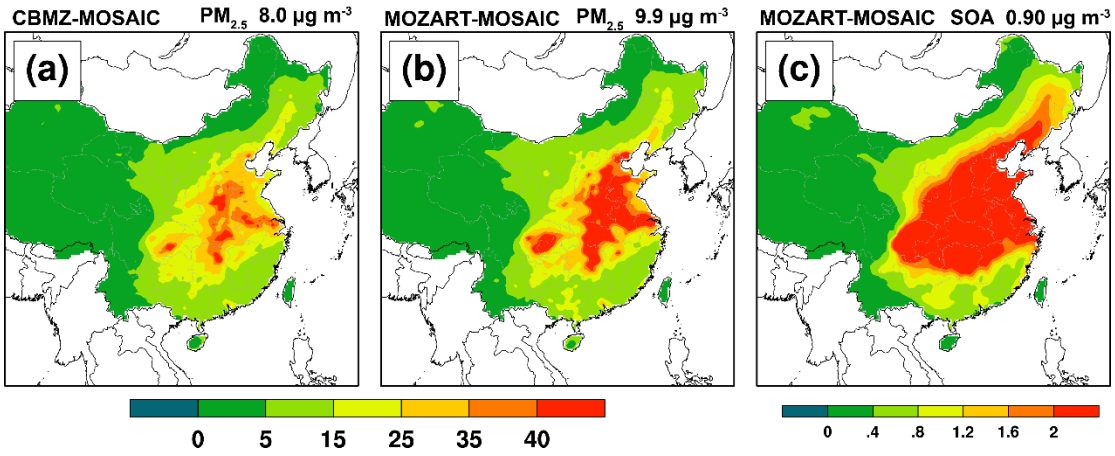

Figure S14. Spatial distributions of simulated mean $PM_{2.5}$ and SOA concentrations (µg m^{-3}) in summer 2017 by **(a)** CBMZ gas-phase chemistry coupled with MOSAIC aerosol module (CBMZ-MOSAIC), **(b, c)** MOZART gas-phase chemistry coupled with MOSAIC aerosol module (MOZART-MOSAIC). The calculated pollutant concentrations averaged over China are also shown at the top of each panel.